BIOCHEMISTRY
including biophysical chemistry & molecular biology

Article

pubs.acs.org/biochemistry

A "Sliding Scale Rule" for Selectivity among NO, CO, and O_2 by Heme Protein Sensors

Ah-Lim Tsai,*[,†] Vladimir Berka,[†] Emil Martin,[‡] and John S. Olson[§]

[†]Division of Hematology, Internal Medicine, University of Texas Medical School at Houston, Houston, Texas 77030, United States
[‡]Division of Cardiology, Internal Medicine, University of Texas Medical School at Houston, Houston, Texas 77030, United States
[§]Department of Biochemistry and Cell Biology, Rice University, Houston, Texas 77251-1892, United States

Supporting Information

ABSTRACT: Selectivity among NO, CO, and O_2 is crucial for the physiological function of most heme proteins. Although there is a million-fold variation in equilibrium dissociation constants (K_D), the ratios for NO:CO:O_2 binding stay roughly the same, 1:~10^3:~10^6, when the proximal ligand is a histidine and the distal site is apolar. For these proteins, there is a "sliding scale rule" for plots of log(K_D) versus ligand type that allows predictions of K_D values if one or two are missing. The predicted K_D for binding of O_2 to *Ns* H-NOX coincides with the value determined experimentally at high pressures. Active site hydrogen bond donors break the rule and selectively increase O_2 affinity with little effect on CO and NO binding. Strong field proximal ligands such as thiolate, tyrosinate, and imidazolate exert a "leveling" effect on ligand binding affinity. The reported picomolar K_D for binding of NO to sGC deviates even more dramatically from the sliding scale rule, showing a NO:CO K_D ratio of 1:~10^8. This deviation is explained by a complex, multistep process, in which an initial low-affinity hexacoordinate NO complex with a measured K_D of ≈54 nM, matching that predicted from the sliding scale rule, is formed initially and then is converted to a high-affinity pentacoordinate complex. This multistep six-coordinate to five-coordinate mechanism appears to be common to all NO sensors that exclude O_2 binding to capture a lower level of cellular NO and prevent its consumption by dioxygenation.

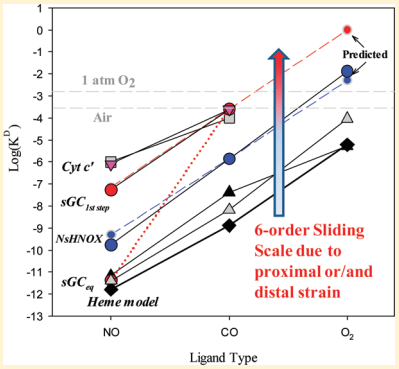

The main biological functions of heme proteins are transport, storage, sensing of key diatomic gaseous molecules, and participation in redox reactions.[1,2] The high reactivity of ferrous heme iron with dioxygen (O_2) to produce radicals precludes its presence as a free form in biological systems to avoid adverse reactions that lead to oxidative stress. Thus, in most cells, free heme is either quickly integrated into proteins or rapidly degraded via the heme oxygenase pathway. The protein not only sequesters the Fe-protoporphyrin ring, but also provides specific axial ligands, steric constraints, and electrostatic interactions that regulate exogenous ligand affinity, heme iron redox potential, and the metal spin state.

Various protein structures have evolved to modulate the intrinsic selectivity of pentacoordinate heme−His complexes for the three major gaseous ligands, nitric oxide (NO), carbon monoxide (CO), and O_2, which differ by only one valence electron between the CO and NO pair and the NO and O_2 pair. The oxygen storage and delivery proteins, Mb and Hb, respectively, use "electrostatic" discrimination to preferentially stabilize bound O_2 via the donation of hydrogen bonds from distal amino acids, normally histidine, tyrosine, or glutamine.[3] In the NO-storing nitrophorins from the saliva of blood-sucking insects, the heme is present in the oxidized form, Fe(III)-protoporphyrin IX, which cannot bind either CO or O_2, but does permit a pH-dependent reversible uptake of NO and displacement by histamine.[4] In the case of FixL, the oxygen sensor found in nitrogen-fixing bacteria, the partial negative charge on bound O_2 induces inward movement of a key Arg220 to form a favorable electrostatic interaction. This conformation change triggers signaling and cannot be achieved by either NO or CO binding because the resulting Fe(II)−ligand complexes lack the strong polarizability of the $Fe(II)^{\delta(+)}-O_2{}^{\delta(-)}$ complex.[5] The CO-sensing protein CooA from phototropic bacteria achieves CO selectivity using a reversible redox switch mechanism. In contrast to reversible CO binding, O_2 binding to CooA causes rapid autoxidation to Fe(III) heme and superoxide formation, and binding of NO leads to dissociation of the proximal ligand. Neither of these latter events triggers signal transduction.[6]

The major target for NO signaling in mammals is sGC, which binds NO, ruptures the proximal Fe−His bond, and triggers activation of cGMP formation. CO binding is weak and not capable of breaking the Fe−His coordination, whereas O_2 simply does not bind to reduced sGC.[7] Most remarkably, sGC manages to bind NO with an apparent K_D of ~4×10^{-12} M (Table 1)[8] but excludes O_2, a property that has not been explained mechanistically. We have addressed this property of sGC quantitatively by defining the general rules that govern

Received: October 10, 2011
Revised: November 22, 2011
Published: November 23, 2011

   dx.doi.org/10.1021/bi2015629 | *Biochemistry* 2012, 51, 172−186

Table 1. Gaseous Ligand Binding Parameter Values for sGC, αβI145Y sGC, Cytochrome *c*′, *Ns* H-NOX, HemAT, Y70F HemAT, Mb, H64V Mb, and Model Heme

sample	K_D (M)	k_{off} (s^{-1})	k_{on} (M^{-1} s^{-1})	refs and comments[a]
wild-type sGC				
NO	4.2×10^{-12},[b] 5.4×10^{-8}[c]	6×10^{-4}, 27[c]	1.4×10^{8},[c] 4.8×10^{8}	8, 9, 22, 4 °C
		~50[d]	2.4×10^{5},[d] 1×10^{6}[e]	8,[d] 4 °C, 9[e]
CO	2.6×10^{-4}	10.7	4×10^{4}	9, 20, 21
O_2	N/A	N/A	N/A	21
cytochrome *c*′				
NO	$1.2–9.1 \times 10^{-6}$	N/D	4.4×10^{4}	24, 25, 27
CO	2.8×10^{-4}	0.028	101	23, 26
O_2	N/A	N/A	N/A	
αβI145Y sGC				
NO	$\leq 0.8 \times 10^{-6}$	≤10	1.2×10^{7}	9
CO	2.5×10^{-4}	0.8	3×10^{3}	9
O_2	N/A	N/A	N/A	9
Ns H-NOX				
NO	1.7×10^{-10}	0.05	3×10^{8}	first 6C NO complex[13]
	0.8×10^{-6}	1.9	2.4×10^{6}	second 6C NO complex[13]
CO	1.4×10^{-6}	3.6	3×10^{6}	6C NO complex[13]
O_2	1.3×10^{-2}[f]	N/A	N/A	slow autoxidation[13]
HemAT				
NO	–	–	–	
CO	1.6×10^{-7}	7.0×10^{-2}	4.3×10^{5}	28
O_2	9.1×10^{-5}	1800	1.9×10^{7}	28
Y70FHemAT				
NO	–	–	–	
CO	6.2×10^{-8}	3.0×10^{-2}	4.7×10^{5}	28
O_2	3.3×10^{-4}	19000	5.3×10^{7}	28
Mb(II), whale				
NO	4.5×10^{-12}	1.0×10^{-4}	2.2×10^{7}	18, 19
CO	3.7×10^{-8}	1.9×10^{-2}	5.1×10^{5}	17, 18
O_2	0.9×10^{-6}	15	1.7×10^{7}	17, 18
H64V Mb				
NO	4.0×10^{-12}	1.1×10^{-3}	2.7×10^{8}	3, 18
CO	6.8×10^{-9}	4.8×10^{-2}	7.0×10^{6}	3, 18
O_2	9.1×10^{-5}	10000	1.1×10^{8}	3, 18
Fe(II)PP(1-MeIm)				
NO	1.6×10^{-12}	2.9×10^{-4}	1.8×10^{8}	14, 16
CO	1.3×10^{-9}	2.3×10^{-3}	1.8×10^{6}	14, 16
O_2	0.6×10^{-5}	310	5.5×10^{7}	15

[a]Unless otherwise specified, the experimental temperature was 20–25 °C. [b]Calculated as k_{off}/k_{on} using values from refs 8 and 34. N/A, not applicable; N/D, not determined. [c]Calculated on the basis of k_{off} and k_{on} for 6c NO complex determined in this study at 24 °C. [d]Ref 8. [e]Ref 9. [f]Determined by an oxygen binding isotherm under high pressure in this study.

ligand selectivity in heme proteins with a neutral proximal histidine–Fe(II) bond. The deviation of the NO binding properties of sGC from these rules requires a multistep binding mechanism, which explains how GC and heme-nitric oxide and oxygen binding (H-NOX) classes of heme-based protein sensors evolved such remarkably high selectivity for NO and against O_2.

To verify the general rules and the multistep mechanism for the NO sensors, we re-examined the first step in binding of NO to sGC and re-evaluated the ligand binding properties of a panel of heme-based protein sensors, globins, and model heme. The almost linear relationship of $\log(K_D)$ for NO versus CO versus O_2 binding for most heme proteins suggests a "sliding scale rule", which allows a prediction of the affinity of one ligand, if K_D for the other ligand(s) is known. Deviations from this sliding scale rule are the result of stereochemical interactions with the surrounding protein elements that enhance selectivity in favor of one of the gaseous ligands and sometimes against the others.

METHODS

Construction of the Expression Vector for His-Tagged *Ns* H-NOX. The H-NOX of *Nostoc* sp. PCC 7120 (*Ns* H-NOX^{-189}) gene sequence (GenBank accession number 17229770) was first optimized for *Escherichia coli* codon usage, replacing several rare codons with high-frequency synonymous codons to form a synthetic gene encoding *Ns* H-NOX. This optimized cDNA, together with six histidine codons inserted upstream of the stop codon (resulting in recombinant *Ns* H-NOX with a C-terminal His tag), was synthesized and cloned into the pBSK vector (Epoch LifeScience, Houston, TX). The *Ns* H-NOX cDNA was released by digestion with NdeI and XhoI and subcloned into pET43.1a (predigested with NdeI and XhoI). The integrity of

dx.doi.org/10.1021/bi2015629 | *Biochemistry* 2012, 51, 172–186

the resulting plasmid, designated pET43.1a-*Ns* H-NOX, was confirmed by restriction digestion and DNA sequencing.

Expression and Purification of His-Tagged Recombinant *Ns* H-NOX, sGC, and Prostacyclin Synthase (PGIS). The *E. coli* C43(DE3)pLysS strain (Lucigen, Middleton, WI) was transformed with the pET43.1a-*Ns* H-NOX expression plasmid and grown overnight in Terrific Broth containing chloramphenicol (45 μg/mL) and ampicillin (150 μg/mL) at 37 °C. The overnight culture (20 mL) was used to inoculate 1 L of Terrifc Broth containing ampicillin (150 μg/mL) and incubated with shaking (200 rpm) at 37 °C until the A_{610} reached 0.8. After the sample had been chilled to 20 °C, heme (2 μM), δ-aminolevulinic acid (0.2 mM), and isopropyl 1-thio-β-D-galactopyranoside (IPTG, 1 mM) were added, and the culture was continued for 48 h at 18 °C with shaking at 200 rpm. Cells were harvested by centrifugation and stored at −76 °C.

Cells from 2 L of culture were resuspended in 125 mL of buffer A [100 mM potassium phosphate (pH 7.5), 100 mM NaCl, 10% glycerol, and 1 mM β-mercaptoethanol]. Egg lysozyme (150 mg in 5 mL of buffer A) was added and the suspension stirred at 4 °C for 1 h, then sonicated (10 min total; 10 s intervals, 50% duty cycle), and then centrifuged at 100000 *g* and 4 °C for 1 h. A 10 mL portion of TALON affinity resin was packed in a glass column (2.8 cm × 23 cm) and washed with 10 volumes of deionized water and 10 volumes of buffer A. The cleared cell lysate containing recombinant *Ns* H-NOX was then added to the column, and the mixture was agitated gently for 2 h at 4 °C on a rotating mixer. The liquid was then drained from the column and the resin washed twice by capping the ends and agitating with 10 volumes of buffer A for 15 min. Then, two similar wash steps were performed with 10 volumes of buffer A containing 5 mM imidazole. The His-tagged *Ns* H-NOX was eluted with 5 volumes of buffer A containing 250 mM imidazole and collected in 3 mL fractions. Fractions containing purified *Ns* H-NOX (based on the A_{418}/A_{280} ratio) were pooled and concentrated with a 30 kDa cutoff Centricon device. The concentrated *Ns* H-NOX was chromatographed on a 10-DG column pre-equilibrated with buffer A to remove imidazole and stored at −76 °C.

Soluble guanylyl cyclase (sGC), with a specific activity of 13.5 μmol of cGMP min^{-1} (mg of sGC)$^{-1}$, was prepared in 50 mM triethanolamine (TEA) (pH 7.5), as previously described.[9] The purified enzyme is 5c ferrous (A_{431} = 110 mM^{-1} cm^{-1}) and is inert to oxygen.

The recombinant human PGIS was prepared as described previously[10] with minor modifications in protein purification.[11] Briefly, the human PGIS cDNA was modified by replacing the hydrophobic amino-terminal segment of the first 17 residues with a seven-residue segment (MAKKTSS) favoring expression in *E. coli* and by adding a four-histidine tag at the carboxyl terminus. The modified cDNA was constructed in the pCW vector driven by *tac* promoter, and recombinant PGIS was purified to electrophoretic homogeneity with a nickel affinity column and CM-Sepharose column chromatography from which PGIS was eluted by 20 mM NaP_i (pH 7.2) containing 150 mM NaCl and 10% glycerol. Purified PGIS was stored at −70 °C. The protein concentration was spectrophotometrically determined using an ε_{418} of 103 mM^{-1} cm^{-1}.

Determination of Protein and Heme Content. The total protein content was assayed with a Bio-Rad *DC* protein assay kit using bovine serum albumin as the standard. The heme content was determined by the pyridine hemochrome method using a difference absorbance coefficient (556−538 nm) of 24.5 mM^{-1} cm^{-1}. All protein samples we used were checked to have a full complement of heme.

Electrophoretic and Immunoblot Analyses. Protein samples were prepared by mixing with electrophoresis sample buffer containing 4.3% SDS and 250 mM dithiothreitol and incubation for 2 at 95 °C. Protein mixtures were separated by electrophoresis under denaturing conditions using 12% polyacrylamide gels, with the protein bands visualized by Coomassie blue staining.

Anaerobic Sequential Stopped-Flow Method. We determined k_{off}(NO) with an Applied Photophysics model SX-18MV stopped-flow instrument with a rapid-scan diode-array accessory. The sample handling unit was located inside an anaerobic chamber (model 110V, Coy Laboratory Products, Inc.) filled with 10% H_2 in N_2 and fitted with a palladium-based O_2 scrubber. A gas analyzer (model 10, Coy Laboratory Products, Inc.) tracked both the hydrogen level and the oxygen level to make sure that the latter is 0 ppm during the kinetic measurements. An sGC solution was prepared in an anaerobic glass titrator via five cycles of vacuum and argon replacement (30 s and 5 min, respectively). A 2 mM NO stock solution and a 1 mM CO stock solution in TEA buffer were prepared in glass tonometers by saturation first with pure nitrogen and then with NO (or CO) at 1 atm. The openings of the side arms of the tonometers were then sealed with a rubber septum, and they were transferred into the anaerobic chamber. An airtight disposable syringe with a needle was used to retrieve different amounts of the NO stock solution to prepare the NO solution used for kinetic measurements. Other details of the kinetic measurements are given in the main text and legend of Figure 2.

Determination of O_2 Binding Affinity for *Ns* H-NOX and sGC under High Pressures. The custom-built pressure cell was equipped with antireflection-coated sapphire windows and had a path length of 1 mm as previously described.[12] In these experiments, 200 μL of the ferrous form of *Ns* H-NOX (50 μM) or sGC (10 μM) was added to the pressure cell that was preflushed with pure oxygen and isolated from air by a screw metal joint and then engaged to the oxygen cylinder by a control valve. The oxygen pressure was varied from 0 to 135 psi (or 9.2 atm) in 20 psi increments. Optical spectra were recorded after each increment of oxygen pressure and equilibration for ∼2 min as the pressurized cell was shaken. After 135 psi, the cell was open to the air pressure and the spectrum was recorded to check the reversibility.

EPR Spectroscopy. Liquid helium-temperature EPR spectra were recorded on a Bruker EMX spectrometer using a GFS600 transfer line and an ITC503 temperature controller. An Oxford ESP900 cryostat was used to accommodate the quartz sample tube in an ER 4116DM resonator.[13] The conditions for liquid helium (10 K) EPR measurements were as follows: frequency, 9.6 GHz; modulation amplitude, 10 G; modulation frequency, 100 kHz; and time constant, 0.33 s.

RESULTS

Linear Logarithm Plots of K_D(NO), K_D(CO), and K_D(O_2) for Heme Proteins with a Neutral Proximal Histidine. Logarithmic plots of equilibrium dissociation constants (K_D), association rate constants (k_{on}), and dissociation rate constants (k_{off}) versus ligand type were constructed for a large series of ferrous heme proteins that contain a neutral proximal histidine ligand (see Figures 1 and 5−8 and Figures S1−S3 of the

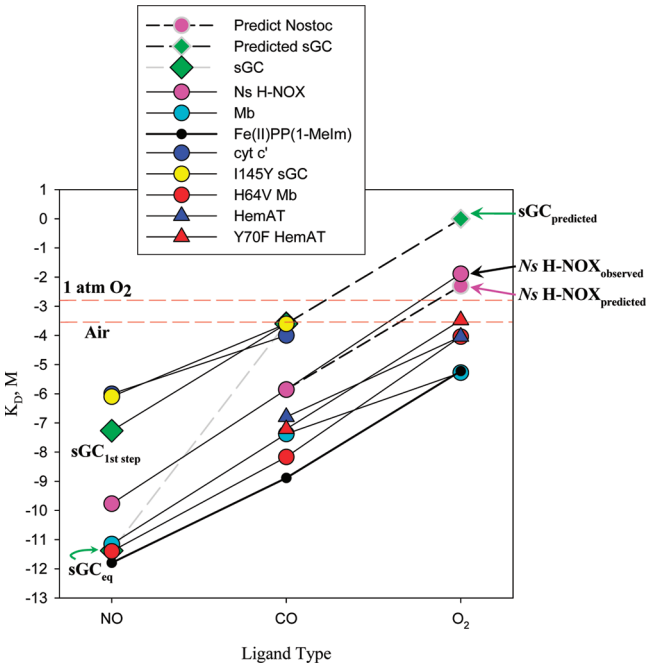

Figure 1. Sliding scale rule relationship of the dissociation equilibrium constants, K_D, of various heme sensors: Fe(II)PP(1-MeIm) (black circles and red line), Mb (cyan circles), H64V Mb (red circles), *Ns* H-NOX (pink circles), cyt *c*′ (blue circles), I145Y sGC (yellow circles), HemAT (blue triangles), Y70F HemAT (red triangles), and sGC (green diamonds). Predicted $K_D(O_2)$ values for sGC and *Ns* H-NOX were obtained by drawing parallel lines from the K_D(CO) to that of the model heme (black dashed lines and symbols with a gray edge). The ~4 order of magnitude difference in K_D(NO) between the 6c and final equilibrium 5c NO complexes formed in sGC is labeled and connected to K_D(CO) (solid vs dotted line).

Supporting Information). In Figure 1, the K_D values for binding of NO, CO, and O_2 to 5c Fe(II)PP(1-MeIm),[14−16] Mb,[17−19] sGC,[8,9,20−22] cytochrome *c*′ (cyt *c*′),[23−27] and HemAT[28] were taken from the literature, and those for sGC containing the I145Y mutation in the β subunit ($\alpha\beta$I145Y sGC)[9] and *Ns* H-NOX[13] were determined by us (Table 1). NO always shows the highest affinity (lowest K_D) because of its radical nature and some back bonding; CO shows an intermediate affinity because of extensive back bonding, and O_2 shows the lowest affinity because only a σ bond can be formed with the iron atom.[29−31] Although the absolute values of K_D vary more than 1 million-fold, i.e., six units along the *y*-axis in Figure 1, the K_D ratios of the CO and NO pair and the O_2 and CO pair for each sample remain between 10^3 and 10^4. This trend is shown most clearly for the Fe(II)PP(1-MeIm) model heme (thick line and small black circles, Figure 1) and leads to a "sliding" set of parallel lines for the NO to CO to O_2 series for most of the proteins that have been examined.

Major exceptions to the linear log plots are observed when hydrogen bond donors are present in the active site, resulting in preferential stabilization of bound O_2 and $K_D(O_2)$ values smaller than those predicted by the sliding scale rule.[3,18] This effect is seen most clearly by the lower than expected $K_D(O_2)$ for wild-type sperm whale myoglobin (swMb) with a distal histidine compared to the higher value for H64V Mb in which the active site is apolar (Figure 1, cyan vs red circles).[32] However, the K_D ratios for the CO and NO pair are relatively unchanged for these Mb variants. Similarly, in HemAT, the distal tyrosine stabilizes bound O_2, and when the tyrosine is replaced with phenylalanine, the apolar HemAT mutant shows a log(K_D) plot perfectly parallel with those for H64V Mb and the model heme (Figure 1, blue vs red triangles).

Thus, for gas-binding heme proteins in the reduced, Fe(II) state, there appears to be a sliding scale rule, which prescribes parallel lines for plots of log(K_D) for the NO to CO to O_2 series. This relationship appears to apply to all 6c heme proteins and model hemes with a neutral proximal histidine ligand, and any decrease in the $K_D(O_2)/K_D$(CO) ratio is readily explained by preferential electrostatic stabilization of the polar Fe−O_2 complex. All other protein structural effects, including direct hindrance of the bound ligand, displacement of water from the active site, and proximal constraints of movements of iron−His species into and out of the plane of the heme, apply

Scheme 1. Mechanism of the Multiple-Step Interaction between NO and sGC[a]

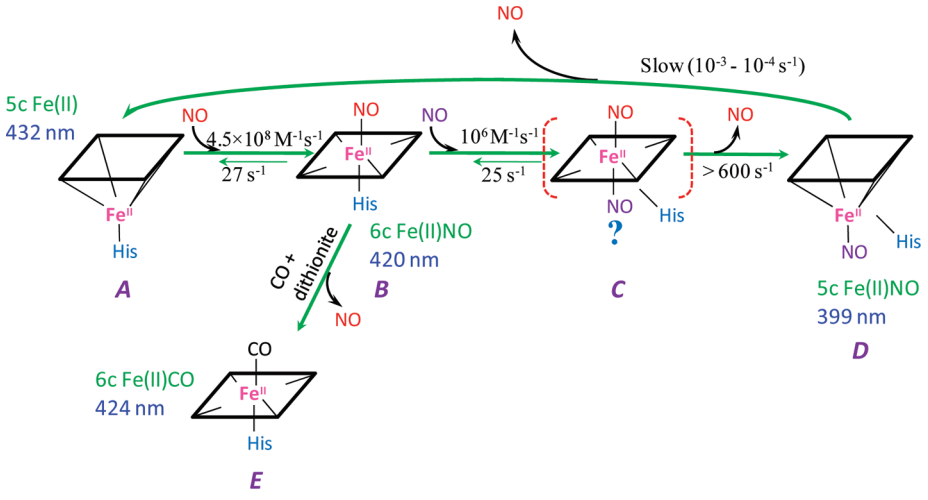

[a]Heme coordination structures and absorption maxima of the 6c CO complex (E) formed in excess CO and dithionite, starting 5c Fe(II)-bound sGC (A), the 6c NO complex (B), and the 5c NO complex at final equilibrium (D) are shown. The proposed transient 6c bis-NO complex (C, in brackets) is supported by the NO concentration dependence of the conversion from B to D and a recent $^{15}NO/^{14}NO$ ligand binding EPR study (E. Martin et al., manuscript in revision). Numbers are rate constants at 24 °C determined in this study and one other recent sGC study.[79]

dx.doi.org/10.1021/bi2015629 | *Biochemistry* 2012, 51, 172−186

uniformly to the binding of all three ligands.[33] The only major exception to this rule is the remarkably large $K_D(CO)/K_D(NO)$ ratio ($\sim 10^7-10^8$) for equilibrium binding to sGC. This ratio is 4−5 orders of magnitude larger than that found for all the other heme proteins that have been examined (Figures 1, 7, and 8 and Figures S1−S3 of the Supporting Information). The binding of CO to sGC is very weak ($K_D \approx 3 \times 10^{-4}$ M), and no binding of O_2 to this protein has been detected. Thus, the predicted K_D for NO binding to form a ferrous 6c complex is $\sim 3 \times 10^{-7}$ to 10^{-8} M based on the sliding scale rule. In contrast, the reported $K_D(NO)$ value based on the ratio of published k_{on} and k_{off} values is 10^{-12} M. This deviation from the sliding scale rule is a consequence of the multistep mechanism for binding of NO to sGC to form a 5c NO−heme complex, as first suggested by Traylor and Sharma (refs 8, 34, and 35) and as has been described by Kruglik et al. (ref 80 and Tsai et al.[13] for Ns H-NOX.

Measurements of k_{on} and k_{off} for the First NO Binding Step for sGC at Ambient Temperature. The k_{off} reported in the literature for dissociation of NO from sGC refers to dissociation of the 5c NO−Fe(II) heme complex in its final equilibrium state (D in Scheme 1) and not to the labile 6c NO−Fe(II)-His complex transiently formed in the first step of NO binding[8,34] (C in Scheme 1). The $k_{off}(NO)$ values for the model heme, all the Mb variants, and the other heme proteins in Table 1 (and Figures 5−7 and Figures S1 and S2 of the Supporting Information) represent the rate of dissociation from bona fide 6c NO complexes. The k_{off} values for initial 6c NO−Fe(II)-His complexes can be reliably measured for cyt c',[24,25] $\alpha\beta$I145Y sGC,[9] and *Ns* H-NOX[13] (Table 1), because in these proteins the initial 6c NO complex is relatively stable and only slowly and partially converts to 5c NO−Fe(II) complexes at low NO:heme concentration ratios.

To resolve the dilemma of the abnormally large $K_d(CO)/K_d(NO)$ of sGC, we determined both the on and off rate constants for the first step of binding of NO to sGC at 24 °C for comparison with the rate constants listed in Table 1, most of which were measured near room temperature. Because the k_{on} value is very large,[8] we had to conduct the kinetic measurements under second-order conditions, using an sGC:NO ratio of 1:1 and a final concentration at 0.5 μM each, to avoid missing most of the time course in the dead time of the stopped-flow apparatus. Measurements performed using either a rapid-scan diode array (Figure 2) or single-wavelength detection (Figure 2, inset) captured more than 60% of the total expected changes. The observed time courses were fitted to a second-order, irreversible mechanism (dashed line in Figure 2, inset) and yielded a k_{on} value of 4.8×10^8 M^{-1} s^{-1}, which is similar to the previously reported value of 1.8×10^8 M^{-1} s^{-1} measured 4 °C.[8]

To accurately measure the k_{off} for the initial 6c NO−sGC complex with a Soret peak at 420 nm, we maximized its formation in sequential stopped-flow mixing experiments. The 6c NO complex was generated by reacting 2 μM sGC with 2 μM NO in the first mixing step. The conversion of Fe(II)-bound sGC to the NO−Fe(II)-His complex (A ↔ B in Scheme 1) was almost complete in the dead time of the stopped-flow apparatus (Figure 3A). This initial NO/sGC mixture was aged for 15−200 ms and then reacted with 1 mM CO and 25 mM dithionite to displace and consume dissociated NO, respectively (B → E in Scheme 1). After the second mixing step, an exponential increase in absorbance at 424 nm was observed, indicating formation of the CO−Fe(II)-His complex (E in

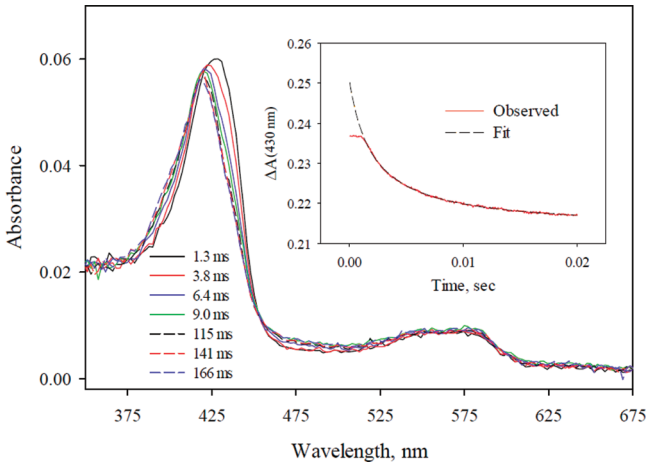

Figure 2. Time-dependent optical spectra of the reaction between 1 μM sGC and 1 μM NO (before mixing) at 23 °C recorded in the anaerobic rapid-scan stopped-flow apparatus. Spectra were recorded at 1.3−166 ms as indicated. Kinetic data of single-wavelength absorbance changes at 430 nm were also recorded (red trace in the inset) and fitted to a true second-order function (black dash in the inset) to obtain the rate constant.

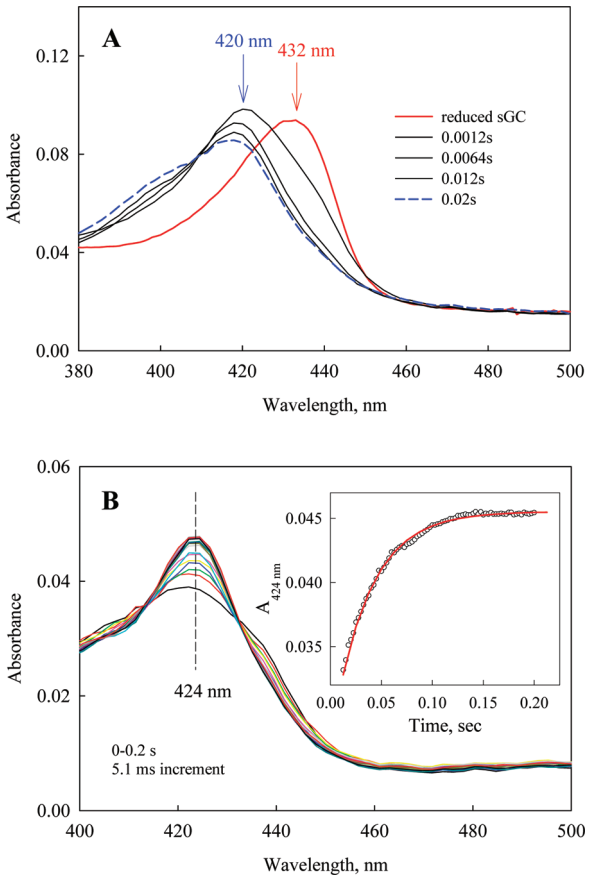

Figure 3. (A) Optical spectral changes during the reaction between sGC and a stoichiometric amount of NO. Rapid-scan stopped-flow data at 23 °C between 3.5 μM Fe(II)-bound sGC and stoichiometric NO were recorded. The peaks of Fe(II), the 6c NO complex, and the 5c NO complex are indicated. (B) Changes in optical spectra upon reaction between 2 μM sGC (premixed with stoichiometric NO) and 1 mM CO with 25 mM dithionite to determine the $k_{off}(NO)$ for the 6c-NO complex. Kinetic data at 424 nm changes with a 20 ms aging time are shown in the inset.

dx.doi.org/10.1021/bi2015629 | *Biochemistry* 2012, 51, 172−186

Scheme 1) with a rate of ~27 s^{-1} (Figure 3B). Increasing the aging time of the original 1:1 sGC/NO mixture to 200 ms led to little variation in the total absorbance change, the final peak position, or the rate of NO displacement (Figure 3B, inset). However, in each case, a small conversion to a 5c NO−Fe(II) complex with a lower-intensity peak at 399 nm (a species similar to D in Scheme 1 but with NO on the distal site of the heme iron) occurs before the 6c NO−Fe(II)-His intermediate is maximally formed. If the same sGC sample is reacted with an excess of NO, a final equilibrium 5c NO−Fe(II) complex is formed rapidly with a 399 nm absorbance band (D in Scheme 1) and little evidence of the 6c intermediates. Reaction of this complex with 1 mM CO and 25 mM dithionite led to a markedly smaller rate of NO dissociation, which is roughly equal to that reported previously in the literature (i.e., ~10^{-4} s^{-1})[36] (D → A in Scheme 1).

The k_{off}(NO) value of 27 s^{-1} for the initial 6c NO complex was used to calculate a K_D(NO) of 5.4 × 10^{-8} M for dissociation of the initial NO−Fe(II)-His complex (Table 1 and Figure 1, green diamonds). When this value for the NO−Fe(II)-His complex of sGC is used, the line connecting log[K_D(NO)] and log[K_D(CO)] becomes parallel with those for all the other heme proteins studied and a 3−4 order of magnitude intrinsic separation of the sGC K_D values between the NO and CO pair. Thus, the sliding scale rule applies for 6c sGC complexes, even though the absolute values of the K_D values for each ligand are ~6 orders of magnitude larger than those for the model heme−imidazole complex.

Linear extrapolation from the log(K_D) values for NO and CO binding predicts a K_D of ~1 M for binding of O_2 to sGC (Figure 1, green diamonds with gray edges), which is 3 orders of magnitude higher than the O_2 concentration in buffer saturated with 1 atm of O_2 (Figure 1, horizontal red dashed lines). Thus, when the 6c sGC complexes are examined, the sliding scale rule predicts the exclusion of oxygen by sGC, and similar empirical predictions can be made for the binding of O_2 to I145Y sGC, cyt *c*′, and *Ns* H-NOX, where the initial 6c NO complexes are more easily examined.

A Test of the Sliding Scale Rule: Binding of O_2 to *Ns* H-NOX under High Pressures. *Ns* H-NOX appears to be unable to bind O_2, but does slowly autoxidize, indicating weak interaction with O_2.[13] Extrapolation from the observed K_D(CO) for *Ns* H-NOX by a line parallel to the data for the other proteins in Figure 1 (pink circles with gray edges) predicts that the K_D(O_2) for this sensor should be ~5 mM. If this prediction of the sliding scale rule is correct, then it should be possible to detect binding of O_2 to *Ns* H-NOX spectrally using only moderately high O_2 pressures. Spectral changes for Fe(II)-bound *Ns* H-NOX were observed in a custom-built pressure cell when P_{O_2} was increased from 0.2 to ~9 atm (130 psi). The Soret band changed from a 430 nm band typical of 5c Fe(II) heme to a broad band centered at 424 nm, which is not the ferric form (Figure 4A). The absorbance difference measured at 409−431 nm depends hyperbolically on O_2 concentration and was consistent in four different experiments. These data were analyzed with a simple one-step binding function, and the fitted K_D of 13 × 10^{-3} M (Figure 4, inset) is close to the value predicted by the sliding scale rule (~5 × 10^{-3} M). In contrast, when the same experiment was attempted with sGC, no change in Soret absorbance was observed, even at 9.2 atm of pure O_2, which is the highest limit before the sample leaks from the pressure cell.

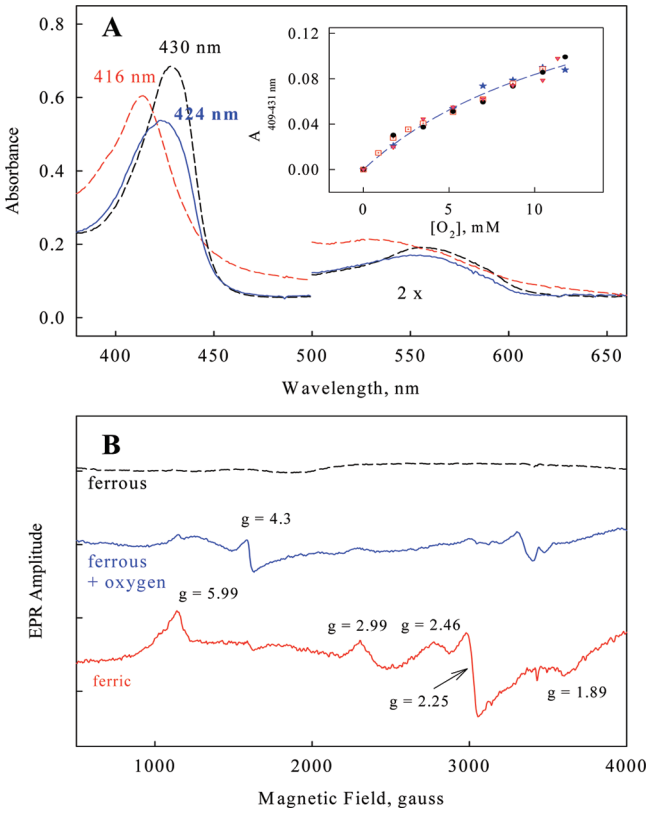

Figure 4. (A) Optical spectra of ferric (red dashed) and ferrous (black dashed) *Ns* H-NOX and ferrous *Ns* H-NOX under 135 psi of O_2 (blue) recorded in a high-pressure cell at 23 °C as described in Methods. (B) EPR spectra of ferric, ferrous, and oxygen-treated ferrous samples in panel A after they had been exposed to the air and transferred into an EPR tube. All samples were at 50 μM. EPR was recorded at 10 K, and the EPR condition is described in Methods.

The lack of a characteristic visible spectrum typical of HbO_2 complexes suggested that some oxidation might have occurred in the *Ns* H-NOX samples, particularly at 9 atm of O_2. EPR spectra of samples withdrawn from the pressure cell were recorded to quantify the amount of iron oxidation (Figure 4B). The oxygenated *Ns* H-NOX sample did exhibit small g = 6 (high-spin) and g = 3 and 2.25 (low-spin) signals for ferric heme and an increased amount of the denatured hemin−protein complex represented by the g = 4.3 signal. However, the majority of the hemes were EPR-silent and present as either 5c Fe(II) or 6c Fe(II)O_2 complexes. Partial autoxidation and irreversible denaturation under treatment with high-pressure O_2 were confirmed by our failure to recover completely the original ferrous spectrum after the high O_2 pressure had been released (data not shown). Nonetheless, it is clear that most of the original unliganded Fe(II)-bound *Ns* H-NOX molecules do reversibly bind dioxygen with a K_D in the range of 5−10 × 10^{-3} M.

Characteristic Dependence of Log(k_{on}) and Log(k_{off}) on Ligand Type. Correlation plots for the logarithms of k_{on} and k_{off} show more complex shapes as a function of ligand type (Figure 5). The log(k_{on}) plots show vertical displacements of a "V-shaped" pattern, with the bimolecular rate constant for CO binding showing the smallest value, which is almost always 100−1000-fold smaller than k_{on}(NO) and 10−100-fold smaller than k_{on}(O_2). As described by Champion, Franzen, Harvey, and their co-workers,[37−40] the much smaller values of k_{on}(CO) are

dx.doi.org/10.1021/bi2015629 | *Biochemistry* 2012, 51, 172−186

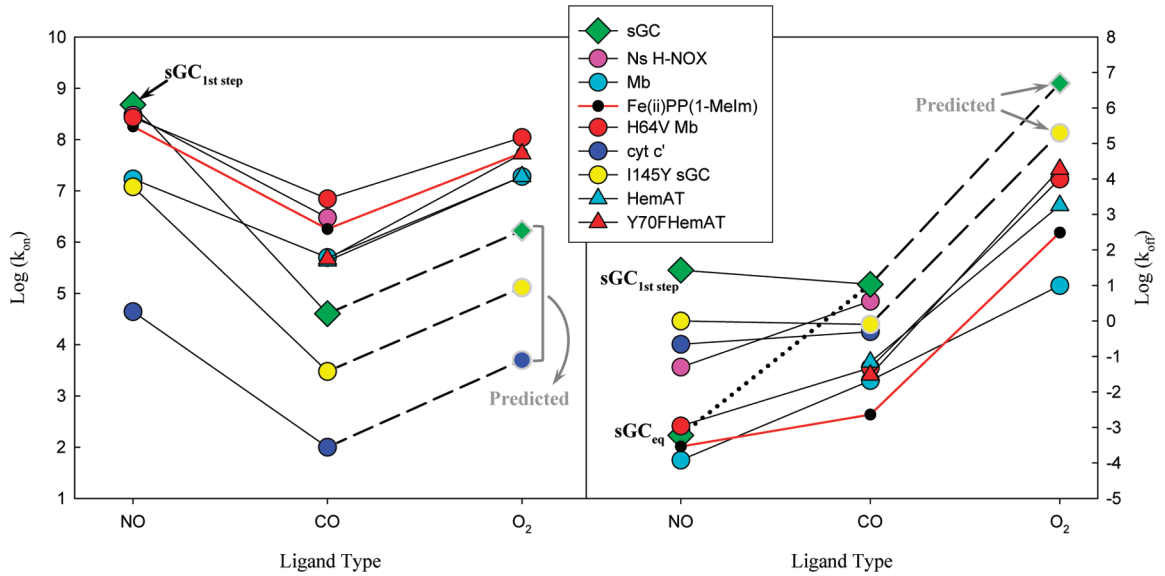

Figure 5. Relationship between log(k_{on}) [or log(k_{off})] values of various heme sensors and three ligand types. The predicted k_{on} (or k_{off}) values are shown by dashed lines and symbols with gray edges. Other features match those in Figure 1.

due to both the requirement of in-plane movement of the heme iron to vacate the electron in the d_{z^2} orbital and the spin-forbidden nature of formation of an iron−carbonyl bond. As a result, the rate-limiting step for CO binding is the formation of an internal bond with the iron atom. In contrast, bond formation can occur without a spin-state change in the iron when NO and O_2 are the ligands, because both contain unpaired electrons.[37−40] As a result, the rate of internal bond formation is very rapid for these ligands, and in the case of NO binding, the rate-limiting step for bimolecular association is migration of the ligand into the active site. In the case of O_2 binding, k_{on} can be limited by both ligand migration and bond formation, depending on the reactivity of the iron atom and steric restriction near the active site.[41] Thus, in most proteins, $k_{on}(NO) \gg k_{on}(CO) < k_{on}(O_2)$ and a sliding V-shaped scale is seen.[41]

The pattern for log(k_{off}) is less clear and shows much great variably in both the $k_{off}(CO)/k_{off}(NO)$ and $k_{off}(O_2)/k_{off}(CO)$ ratios. However, in general, $k_{off}(NO) \leq k_{off}(CO) \ll k_{off}(O_2)$, so the pattern has characteristics of a "backward L". In general, the rate constant for O_2 dissociation in heme proteins with an apolar active site is roughly 10^6-fold greater than that for CO dissociation, and assuming this relationship holds for gas sensors, the predicted O_2 dissociation constant for sGC is estimated to be $\sim 5 \times 10^6$ s^{-1} (Figure 5, right panel, dashed line and green diamonds with gray edges vs red line and black circles). The $k_{on}(O_2)$ for sGC can then be estimated from this predicted k_{off} and the estimated K_D (~1 M) from Figure 1. The resulting k_{on} value is $\sim 2 \times 10^6$ M^{-1} s^{-1} (Figure 5, left panel, green diamonds with gray edges), conforming well with the expected V shape for log(k_{on}) plots.

Are the Sliding Scale Rules Applicable to All Globin Variant? Over the past 20 years, the biochemical mechanisms for NO, CO, and O_2 binding have been examined systematically for large libraries of mammalian Mb and Hb variants.[3,32,33] As a test of the analysis in Figure 1, we constructed a graphical analysis for binding of NO, CO, and O_2 to 11 single Mb mutants, from a panel of 42 for which we have complete binding parameter values.[42−44] These 11 Mb mutants showed the largest changes in K_D, k_{on}, or k_{off} compared to the wild-type (wt) Mb parameters. As shown in Figure 6A, the $K_D(NO)$ and $K_D(CO)$ values for these 11 mutants are highly correlated in the ranges of 10^{-10}−10^{-12} and 10^{-7}−10^{-9} M, respectively, showing parallel lines in the log plots.

In contrast, the log[$K_D(O_2)$] values show significant deviations from the linear sliding scale rule. Marked decreases in $K_D(O_2)$ are observed for those variants with an increased level of hydrogen bonding or favorable positive electrostatic fields, which preferentially stabilize bound O_2 (i.e., variants with His64 and Phe29). However, those Mb mutants with apolar distal pockets follow the expected linear sliding scale rule (Figure 6A, thick blue lines). The *y*-axis positions of the log(K_D) values can be readily interpreted in terms of structural effects that regulate ligand affinity, all of which have been well-established for Mb[3,32] and are indicated by the arrows in Figure 6. Lower iron reactivity due to proximal constraints of in-plane movement, direct steric hindrance at the active site, and displacement of water from the distal pocket increase the K_D for the binding of all three gaseous ligands, whereas positive fields and hydrogen bond donors preferentially stabilize bound O_2, causing a downward deflection of the last log[$K_D(O_2)$] points in the plots (Figure 6A). Similar trends and explanations apply to all the other Mb variants that have been examined, and examples of these data are shown in Figures S1A and S2A of the Supporting Information for double and triple mutants.

Correlation plots for the bimolecular association (k_{on}) and unimolecular dissociation (k_{off}) rate constants for the same set of reduced Mb variants are shown in Figure 6B. The trends for log(k_{on}) are given in the left-hand panel, and the V shape is result of the differences in rate-limiting steps. Binding of NO to ferrous deoxyMb is limited only by the rate of entry into the protein active site; CO binding is limited by bond formation, and O_2 binding is partially limited by both processes. The bimolecular rate of ligand entry is governed by displacement of distal pocket water, diffusion into the distal pocket, and the size of the internal capture volume, whereas the rate of bond formation is governed by the reactivity of the iron atom (proximal effects) and steric hindrance at the open axial position. In the case of CO binding, the overall expression for k_{on} is $k_{bond}K_{entry}$, where K_{entry} is the equilibrium constant for

dx.doi.org/10.1021/bi2015629 | *Biochemistry* 2012, 51, 172−186

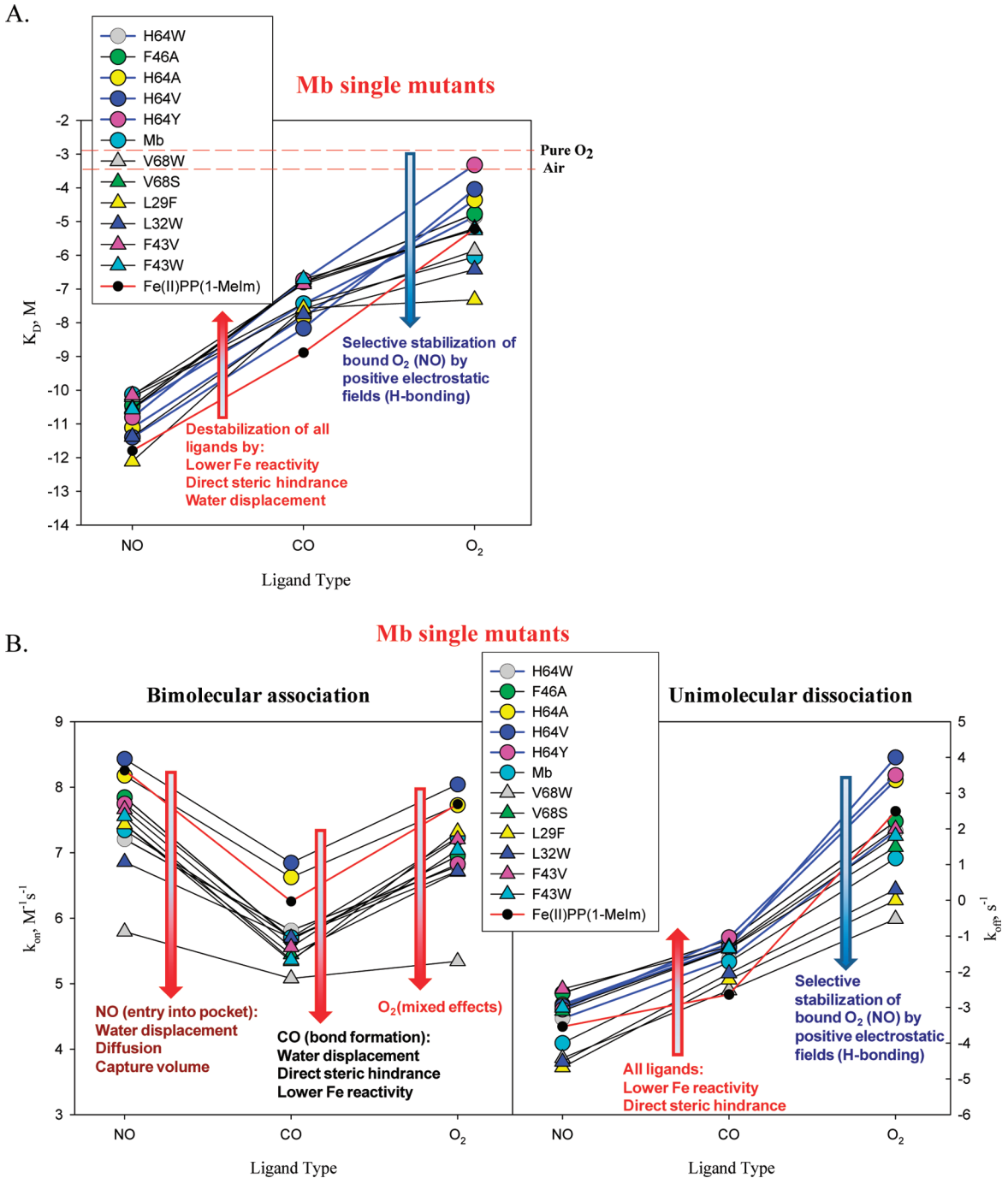

Figure 6. Categorical plot of either log(K_D) (A) or log(k_{on}/k_{off}) (B) vs ligand type similar to Figure 1 for a panel of single mutants of Mb together with the model heme control (red line and black circles). Blue thick lines indicate the data of mutants with the key His64 changed to other residues. Binding parameter values are summarized in Table S1 of the Supporting Information.

noncovalent ligand binding in the active site, which also depends on the need to displace distal pocket water and the active site volume.[41] Thus, when iron reactivity is lowered by proximal effects or direct hindrance, the depth of the V shape in the log(k_{on}) plot is greater because of the slight changes in k_{on}(NO) but large decreases in k_{on}(CO). However, if the capture volume is decreased markedly as is the case for V68W Mb, all the rates are decreased dramatically and the V shape is much more shallow because slow ligand capture becomes limiting for all three ligands (Figure 6B, left panel, gray triangles).

The dominant variations seen in the log(k_{off}) plots are due to preferential electrostatic stabilization of bound O_2, causing dramatic decreases in the absolute value of $k_{off}(O_2)$ and the $k_{off}(O_2)/k_{off}$(CO) ratio (Figure 6B, right panel). In contrast, decreases in Fe(II) reactivity and direct steric hindrance of the bound ligand cause increases in k_{off} for all three ligands. There is some variability in k_{off}(NO) because the Fe(II)NO complex can be stabilized weakly by hydrogen bonding.[3,45] Again, similar correlation plots and interpretations can be made for libraries of double and triple mutants of sperm whale Mb, and the results

dx.doi.org/10.1021/bi2015629 | *Biochemistry* 2012, 51, 172−186

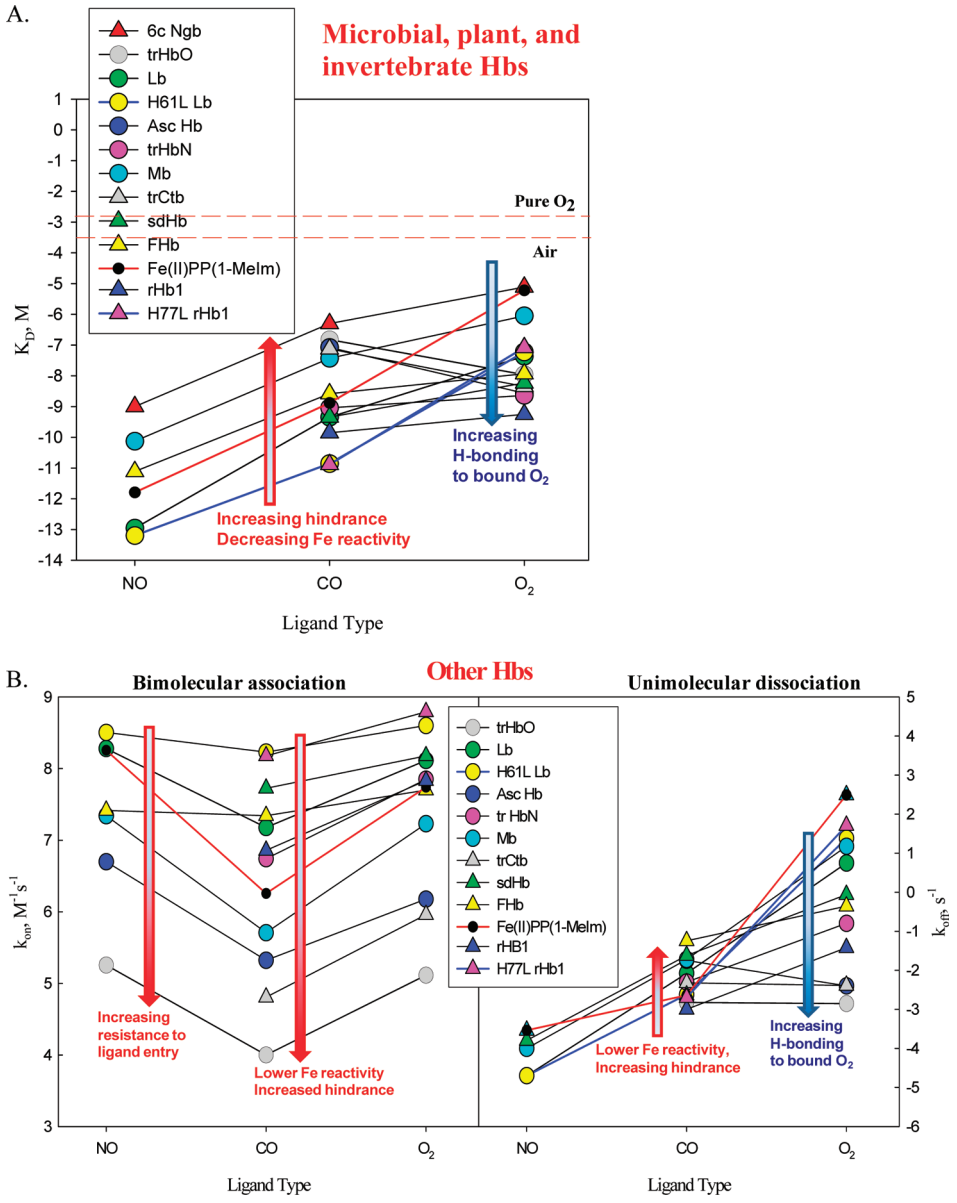

Figure 7. Categorical plot of either log(K_D) (A) or log(k_{on}/k_{off}) (B) vs ligand type conducted for several globins: leghemoglobin (Lb, green circles) and its H61L mutant (yellow circles), rice hemoglobin type 1(rHb1, blue triangles) and its H77L mutant (red triangles), Hb from *A. suum* (Asc Hb, blue circles), flavohemoglobin (FHb, yellow triangles) from bacteria and fungi, truncated Hb (trHb) from microorganisms, including trHbN (pink circles) and trHbO (gray circles) from *M. tuberculosis* and trCtb (gray triangles) and sdHb (green triangles) from *C. jejuni*. and even the 6c neuroglobin (Ngb, red triangles) together with Mb (cyan circles) and the model heme control (red line and black circles). Blue thick lines indicate the data of mutants with the key His64 changed to other residues. Binding parameter values are summarized in Table S2 of the Supporting Information.

all support the sliding scale rules (Figures S1 and S2 of the Supporting Information).

As a more stringent test of the sliding scale analyses, we examined the ligand binding parameters for 11 different reduced globins from all kingdoms of life, including the plant hemoglobins, leghemoglobin (Lb)[46] and rice hemoglobin 1 (rHb1);[47] the invertebrate Hb from *Ascaris suum* (Asc Hb);[19] flavohemoglobins (FHb) from bacteria and fungi; truncated Hbs (trHbs) from microorganisms, including trHbN and trHbO from *Mycobacterium tuberculosis* and trCb, a single-domain hemoglobin from *Campylobacter jejuni*;[48] and human neuroglobin (Ngb)[49] (Figure 7 and Table S2 of the Supporting Information). There is a much greater range of absolute values for all the rate and equilibrium parameters, but the same rules and interpretations apply. For some of these globins, there are multiple hydrogen bonding interactions with bound O_2 leading to dramatic decreases in $K_D(O_2)$ and $k_{off}(O_2)$ and $K_D(O_2)/K_D(CO)$ and $k_{off}(O_2)/k_{off}(CO)$ ratios of ≤1.0 (i.e., *Ascaris* Hb, trHbO, trHbN, rHb1, and trCb). When the active site proton donors are replaced with apolar amino acids, the expected linear, V-shaped, and reverse L-shaped plots are observed for log(K_D), log(k_{on}), and log(k_{off}), respectively (Figure 7, thick blue lines). These data, coupled with those for the Mb libraries and the heme proteins shown in Figure 1, argue strongly for the utility of the sliding scale analysis and its ability to predict ligand binding parameters, if a set of K_D, k_{off}, and k_{on} parameters have been measured for CO binding and the polarity of the active site is known.

dx.doi.org/10.1021/bi2015629 | *Biochemistry* 2012, 51, 172−186

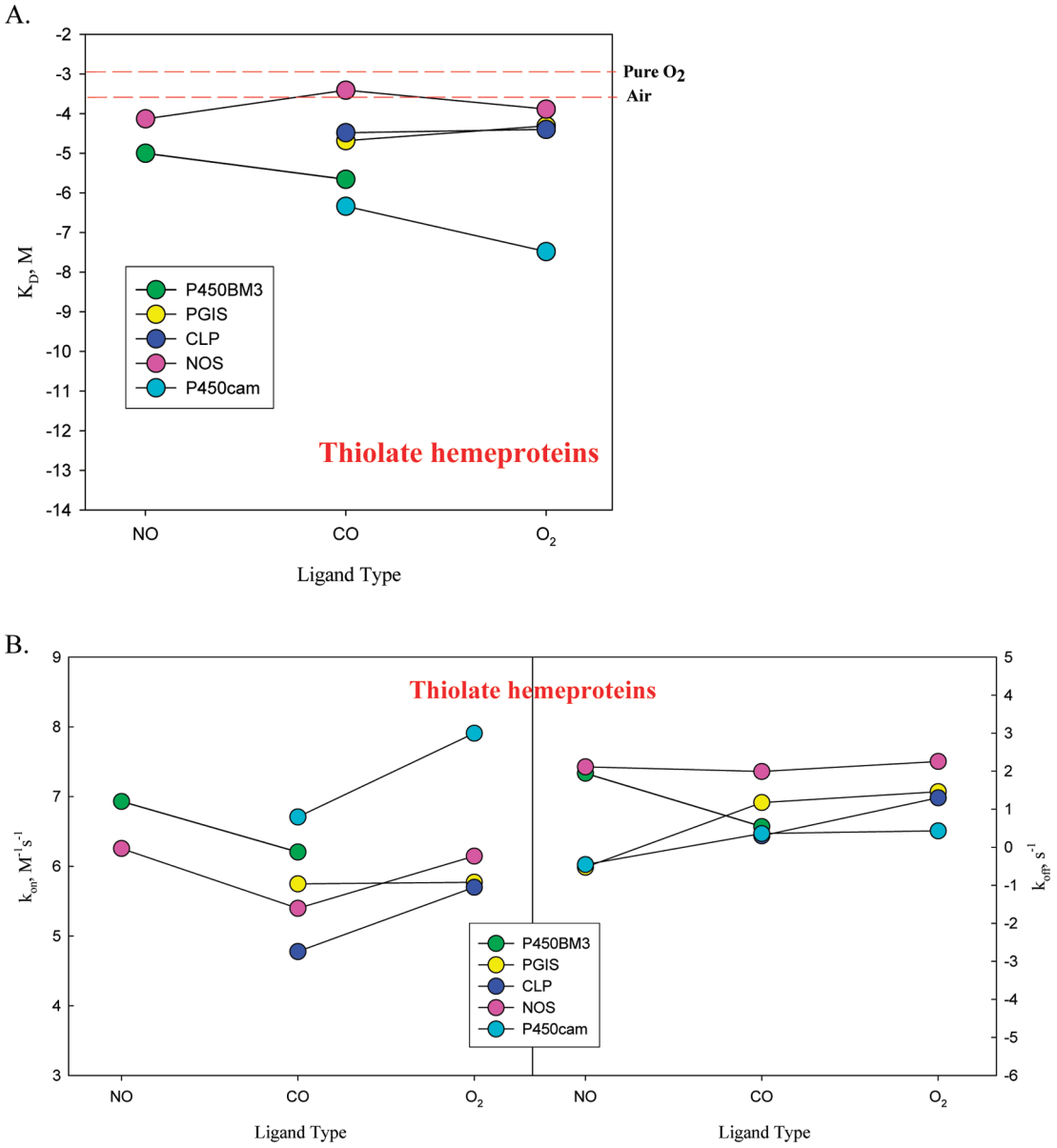

Figure 8. Categorical plot of either log(K_D) (A) or log(k_{on}/k_{off}) (B) vs ligand type for several hemoproteins containing a thiolate proximal ligand, including cytochrome P450BM3 (green circles), prostacyclin synthase (PGIS, yellow circles), chloroperoxidase (CLP, blue circles), nitric oxide synthase (NOS, pink circles), and P450cam. Binding parameter values are summarized in Table S3 of the Supporting Information.

Heme Proteins with a Thiolate Proximal Ligand Do Not Follow the Sliding Scale Rule. There are limited and, in most cases, incomplete kinetic data for binding of NO, CO, and O_2 to the reduced form of cytochrome P450 and P450-like proteins containing a proximal thiolate protein ligand. Nitric oxide synthase is the only one with a complete set of published binding parameters for all three ligands[50,51] (Table S3 of the Supporting Information). K_D and k_{on} values for only two gas ligands are available for Fe(II)-bound P450cam,[52−54] P450BM3,[54,55] chloroperoxidase (CLP),[56,57] and prostacyclin synthase (PGIS).[58,59] The k_{on}(NO) values for both P450cam and PGIS are $\gg 10^8$ M^{-1} s^{-1} (R. Van Eldik, personal communication, and our unpublished results, respectively) and cannot be determined by simple rapid-mixing methods; however, the k_{off}(NO) values could be determined for these two proteins. The ferric P450cam−NO complex was reduced with excess $[Ru(EDTA)H_2O]^-$, and k_{off}(NO) was determined to be 0.35 s^{-1}.[52] For PGIS, the ferrous protein was prepared by anaerobic titration with dithionite, and k_{off} was measured by sequential mixing, stopped-flow protocols, as described for measuring k_{off}(NO) for the 6c NO complex of sGC (see Methods and Figure 3). A delay time of 0.5−1 s allowed us to maximize formation of the Fe(II)NO complex before the ligand was displaced by mixing with 1 mM CO and 40 mM dithionite. The kinetics of dissociation of CO from the ferrous PGIS−CO complex was determined to be 0.3 s^{-1} at 24 °C by mixing with buffer equilibrated with 1 atm of NO (Figure 8B, right).

Even with limited data, it is clear from Figure 8A and Table S3 of the Supporting Information that the log(K_D) values for heme proteins with a proximal thiolate fail to follow the simple sliding scale rule observed for proteins with a proximal His (Figures 1 and 5−7). There is little variation in the K_D values for all three ligands, and $K_D(O_2)$ is actually smaller than K_D(CO) for P450cam, even though there are no polar residues

dx.doi.org/10.1021/bi2015629 | *Biochemistry* 2012, 51, 172−186

in the active site to stabilize bound dioxygen (Table S3 of the Supporting Information). Thiolate coordination seems to abolish ligand binding selectivity. With the exception of that of PGIS, the k_{on} values seem to still follow the V shape sliding scale rule (Figure 8B, left panel), but the reversed L sliding scale relationship no longer holds for k_{off} values for P450-like heme proteins, for which there is a leveling effect causing the k_{off} values of all three ligands to be very similar (Figure 8B, right panel).

Peroxidases Also Do Not Follow the Sliding Scale Rules. We also analyzed data for five peroxidases, which have published binding parameters for at least two of the gas ligands (Table S4 of the Supporting Information). These enzymes include horseradish peroxidase (HRP),[60,61] lactoperoxidase (LPO),[62,63] eosinophil peroxidase (EPO),[62] cytochrome *c* peroxidase (CcP),[64,65] and myeloperoxidase (MPO).[62,66] In these proteins, the anionic imidazolate form of the proximal His side chain is coordinated to the iron atom due to the presence of ionized Asp and Glu side chains.[67] Plots of $\log(K_D)$ versus ligand type for these enzymes show little variation and look similar to those for the P450-like heme proteins with a thiolate axial ligand (Figure S3A of the Supporting Information). The $\log(k_{on})$ values still show a V-shaped dependence but are clustered in a very narrow range for all three k_{on} parameters with values that are ~3 orders of magnitude lower than those for the chelated model heme (Figure S3B of the Supporting Information, left). The $\log(k_{off})$ plots show both $k_{off}(NO)$ and $k_{off}(O_2)$ values that are greater than the $k_{Off}(CO)$ values, a behavior that is different from that of heme proteins with a neutral proximal imidazole axial ligand and the P450-like proteins with a thiolate ligand. More work is needed to understand the structural and chemical bonding mechanisms that regulate binding of gas to the latter two classes of heme proteins.

DISCUSSION

Utility of the Sliding Scale Analysis for Understanding Ligand Discrimination. Reduced pentacoordinate heme proteins with a neutral proximal histidine show innate chemical discrimination among NO, CO, and O_2, just like the Fe(II)−imidazole heme model, even though the absolute affinities for any specific ligand can vary more than 1 million-fold (Figure 1). Extensive back bonding from the exogenous ligand to the iron d orbitals is allowed by the neutral axial imidazole and, coupled with the radical nature of NO, causes the K_D for NO binding to be roughly 10^{-3}−10^{-4}-fold smaller than that for CO binding, which in turn is 10^{-3}−10^{-4}-fold smaller than that for the binding of O_2, which lacks the ability to back bond. Thus, plots of $\log(K_D)$ versus ligand type for NO, CO, and O_2 are roughly linear and parallel for a wide variety of heme models and proteins that have apolar active sites and a neutral proximal histidine (Figures 1, 6, and 7). Studies of ligand binding parameters for synthetic model hemes designed to modulate the steric and electrostatic interaction seen in proteins are sporadic and incomplete[14−16,68−72] (Table S5 of the Supporting Information). We could not find another model heme compound, containing a proximal imidazole ligand, for which binding kinetic studies had been conducted with all three gases. Most experiments examined only O_2 and CO binding (e.g., ref 68) and were limited to compounds containing a proximal imidazole base.[14−16,71,72] However, the data that do exist show the general relationship $K_D(O_2)/K_D(CO) \approx 10^3$−$10^4$ for models with apolar distal regions, and this ratio is relatively insensitive to the degree of steric hindrance as indicated by a series of heme models with picket fence, strapped, pocket, and capped distal pockets (Table S5 of the Supporting Information).[68,71,73−75] Only polar interactions or a severe steric effect that led to substantial porphyrin nonplanarity led to a marked lowering of this ratio.[68,71,73−75]

This linear relationship suggests a sliding scale along the *y*-axis of these plots and preservation of marked ligand discrimination, with the relative affinities always being in the following order: NO ≫ CO ≫ O_2. The absolute affinity can be increased by facilitating or sterically pushing the proximal Fe−imidazole complex into the plane of the porphyrin ring to enhance the reactivity of the iron atom and/or by removing any steric constraints adjacent to the distal axial position. These structural effects in combination with the intrinsic chemical differences between the ligands lead to a remarkably wide range of ligand affinities, from 10^{-13} to almost 1 M (Figures 1 and 7). This combination of ligand discrimination coupled with a much wider range of possible ligand binding affinities accounts for why gas sensor, storage, and transport heme proteins maintain the neutral form of the proximal imidazole.

In contrast, when the proximal ligand is a thiolate (P450-like heme proteins) or an imidazolate (peroxidases), there is very little equilibrium discrimination among NO, CO, and O_2, and the range of absolute affinities is smaller, with K_D values ranging from 10^{-7} to 10^{-3} M. Thiolate is a very strong field ligand and highly electron-donating. As a result, there is strong competition for back bonding to the Fe(II) d_{z^2} orbital with the distal gaseous ligand.[31] This competition with the thiolate exerts a leveling effect among NO, CO, and O_2 and, in general, decreases the Fe−XO bond strength and increases both the K_D and the k_{off} for all three gaseous ligands (Figure 8). Similar interpretations apply to peroxidases containing a proximal imidazolate ligand (Figure S3 of the Supporting Information). HRP, LPO, CcP, ascorbate peroxidase, lignin peroxidase, and peanut peroxidase all have a proximal histidine with imidazolate character due to H-bonding interactions with nearby proton bond acceptors (Asp or Asn).[67] These peroxidases all have negative midpoint potentials, and the strong electron donating or pushing effect by the imidazolate helps promote heterolytic cleavage of the O−O bond of bound peroxide, but at the expense of much weaker discrimination between the gaseous ligands and higher K_D values. Although crystallographic data for EPO are not available and MPO has an abnormally high midpoint potential and weak affinity for CO, biophysical studies have demonstrated that both peroxidases still have an imidazolate, proximal ligand,[67] accounting for their lack of discrimination between the gaseous ligands.

The sliding scale rule is also useful for predicting K_D values that are difficult or impossible to measure experimentally. Several NO-sensing heme proteins show very little or no reactivity toward O_2, making it difficult to even estimate $K_D(O_2)$. However, it is straightforward to measure $K_D(CO)$ values for these proteins (Table 1 and Figure 1). If the sliding scale rule applies, the slopes of $\log(K_D)$ versus ligand plots for model hemes or other proteins can be used to predict $K_D(O_2)$ values for the NO sensors. This analysis is shown in Figure 1 for *Ns* H-NOX and sGC, and the predicted K_D values are ~0.005 and ~1 M, respectively. As shown in Figure 4, binding of O_2 to *Ns* H-NOX can be observed at high pressures, and the fitted value for $K_D(O_2)$ was ~0.010 M, which on a logarithmic scale is very close to the predicted value and verifies the utility of the sliding scale rule. The value for sGC shows that it would

require ≥100 atm of pure O_2 for the observation of any binding at all (i.e., ≥10% saturation), which accounts for why no O_2 binding has been observed and autoxidation occurs in days.

The sliding scale rule can also be used to predict K_D(NO) values of ~10^{-8} and ~10^{-10} M for sGC and *Ns* H-NOX, respectively, based on the measured K_D(CO) values for these NO sensors. Again, the predicted value for *Ns* H-NOX agrees well with that measured for the formation of the first 6c NO complex,[13] verifying our analysis. In contrast, the reported K_D for binding of NO to sGC is ~1×10^{-12} M, which is almost 10000-fold smaller than the predicted value. However, the final sGC form is a 5c NO−heme complex with the proximal imidazole displaced. Thus, both the lack of correlation with the sliding scale rule and the change in proximal coordination geometry indicate a complex, multiple-step mechanism for binding of NO to sGC. Nonetheless, as shown in Figures 2 and 3, the first NO binding step to form a transient 6c NO−heme−neutral imidazole complex shows a K_D of 5×10^{-8} M, which is remarkably close to the value predicted from the sliding scale rule and again verifies its utility.

Oxygen Sensor, Storage, and Transport Heme Proteins. Specific high-affinity O_2 binding requires significant deviation from the sliding scale rule both to alter ligand discrimination and to decrease $K_D(O_2)$ values into the micromolar range for sensing, transport, and storage and to the nanomolar range for O_2 scavenging without oxidation. As described in previous work,[32,76] selective increases in O_2 affinity are achieved by increased positive electrostatic fields adjacent to the Fe−O_2 complex and direct hydrogen bonding. As shown in Figures 1, 6, and 7, these favorable polar interactions can decrease the $K_D(O_2)/K_D$(CO) ratio from ~10000 for apolar active sites to ≤1.0 in proteins where multiple hydrogen bonds are donated to bound O_2. The best example of a heme protein with a nanomolar $K_D(O_2)$ and little or no CO binding is the domain 1 hemoglobin of *A. suum*, which is an obligate anaerobe in its adult stage and requires this globin to protect itself from O_2 poisoning (Figure 7 and ref 19). The sliding scale rule analyses in Figures 6 and 7 provide a concise way of quantifying and comparing the effects of distal pocket polarity on discrimination in favor of O_2 binding.

NO Sensors and Discrimination against NO Dioxygenation. In the case of NO sensors, the problem is not equilibrium ligand discrimination. All proteins with a neutral proximal histidine and an apolar distal pocket have much higher affinities for NO than for either CO or O_2. Even in air (2.5×10^{-4} M O_2) and low levels of NO (10^{-9} M), the $K_D(O_2)/K_D$(NO) ratio of 10^8 still favors reversible NO binding. The dilemma is NO dioxygenation by bound O_2, which destroys the signaling molecule. In air and low levels of NO, O_2 will kinetically outcompete NO for initial binding to 5c Fe(II)-bound unliganded heme protein sensors because the values of $k_{on}(O_2)$ are normally only slightly smaller than those of k_{on}(NO) (Figures 5−7). Then NO will react rapidly with the newly formed O_2−heme−imidazole complex to produce nitrate with a bimolecular rate constant roughly equal to that for simple binding of NO to the unliganded protein.[77,78] Thus, for a NO sensor to remain functional under aerobic conditions, it has to completely exclude O_2 binding to prevent NO dioxygenation. This requirement has been achieved in *Ns* H-NOX, cyt *c*′, and sGC by combinations of proximal restrictions and steric hindrance of the bound ligand, both of which markedly reduce ligand affinity. However, these structural effects also markedly increase the K_D for NO binding to form a conventional 6c NO−heme−imidazole complex (Scheme 1 for sGC). On the basis of the sliding scale rule, the CO binding parameters for sGC predict a K_D(NO) value in the 10^{-8} M region, which is too high for sensing nanomolar levels of the gas. Thus, sGC has evolved a complex multistep reaction mechanism in which the initial 6c NO complex converts to a high-affinity 5c complex by displacement of the proximal imidazole, a process that is accelerated by additional NO molecules (Scheme 1 and refs 27 and 79). The net result is a picomolar affinity of NO for sGC and total exclusion of O_2 binding even under aerobic conditions. Similar multistep NO reactions and O_2 exclusion were also observed for cyt *c*′, which shows high selectivity for NO.[80] In this protein, O_2 binding is excluded by distal steric hindrance from the L16 side chain[26,27] rather than the proximal strain as shown for sGC.

The nitrophorin NO-storing protein found in insect salivary glands has adopted an alternative mechanism for preventing O_2 binding and dioxygenation. Nitrophorins exist in the Fe(III) state, which excludes O_2 and CO binding, but can still bind NO, although with only micromolar K_D values. The high K_D facilitates rapid displacement of NO by histamine after injection into mammalian hosts, which induces vasodilation and inhibits inflammation at the same time. This strategy of using Fe(III) binding is effective for NO storage and rapid release at high concentrations but not for sensing nanomolar levels of NO as a cell signaling molecule.

CONCLUSIONS

Five-coordinate Fe(II) heme proteins with a neutral proximal His ligand strongly discriminate between the gaseous ligands, with affinities in the order NO ≫ CO ≫ O_2 due to differential effects of back bonding and spin coupling. There is a linear dependence of log(K_D) on ligand type for the NO, CO, and O_2 series, regardless of the absolute values for individual equilibrium dissociation constants. Deviations from this sliding scale rule do occur in heme proteins that function as relatively high-affinity O_2 sensors, storage proteins, and transport proteins and have active site amino acids that can donate hydrogen bonds to the bound O_2 molecule and preferentially lower $K_D(O_2)$. Cytochrome P450-like proteins and peroxidases contain strong field proximal thiolate and imidazolate ligands, which assist in heterolytic O−O bond cleavage of the substrate but compromise their ability to discriminate among NO, CO, and O_2 binding. NO sensor proteins restrict the binding of all gaseous ligands by both proximal constraints of in-plane iron movement and direct hindrance of the bound ligand. These constraints effectively exclude O_2 binding. High affinity for NO is achieved by a second step in which an ultrastable 5c NO−heme complex is formed by displacement of the proximal His. This multistep mechanism appears to be a general strategy for all high-affinity NO sensors that need to exclude O_2 binding to prevent dioxygenation of the signaling molecule.

ASSOCIATED CONTENT

Supporting Information

Binding parameter values for NO, CO, and O_2 of Mb single mutants (Table S1), other globins (Table S2), heme proteins containing a thiolate proximal ligand (Table S3), heme proteins containing a proximal imidazolate ligand (Table S4), and a panel of picket fence, pocketed, strapped, and capped heme models (Table S5) and correlational plots between binding parameters and ligand types for the Mb double mutants (Figure S1), triple mutants (Figure S2), and peroxidases with

imidazolate proximal ligands (Figure S3). This material is available free of charge via the Internet at http://pubs.acs.org.

AUTHOR INFORMATION

Corresponding Author

*Division of Hematology, Internal Medicine, University of Texas Medical School at Houston, MSB 5290, 6431 Fannin, Houston, TX 77030. Phone: (713) 500-6771. Fax: (713) 500-6810. E-mail: Ah-lim.tsai@uth.tmc.edu.

Funding

This work was supported by National Heart, Lung, and Blood Institute Grants HL095820 (A.-L.T.), HL088128 (E.M.), and HL047020 (J.S.O.), National Institute of General Medical Sciences Grant GM035649 (J.S.O.), the American Heart Association, South Central Affiliate, Grant-in-Aid 09GRNT2060182 (E.M.), and The Robert A. Welch Foundation Grant C-0612 (J.S.O.).

ACKNOWLEDGMENTS

We thank Dr. Lee-Ho Wang for providing us with a prostacyclin synthase sample for NO binding kinetic measurements and Dr. Wen Liu for establishing the expression system for *Ns* H-NOX and purifying the recombinant protein for our oxygen binding experiment. We also thank Professor Joseph Bonaventura for suggesting that we try high-pressure cell binding of O_2 to the sensors at the Gordon Research Conference on Nitric Oxide, 2011. Finally, we acknowledge the strong influence that Vijay S. Sharma and Teddy G. Traylor had on our thinking about ligand discrimination and binding of NO to heme proteins. Their ideas published and shared with one of us (J.S.O.) in the late 1980s were among the first to recognize the importance of distal pocket polarity in preferentially stabilizing bound O_2 in globins and the formation of pentacoordinate NO−heme complexes in NO sensors.

ABBREVIATIONS

NO, nitric oxide; CO, carbon monoxide; O_2, dioxygen; DTT, dithiothreitol; β-BME, mercaptoethanol; IPTG, isopropyl 1-thio-β-D-galactopyranoside; cGMP, cyclic GMP; Mb, myoglobin; Fe(II), ferrous heme; Fe(III), ferric heme; 5c, five-coordinate; 6c, six-coordinate; 5c-NO, five-coordinate NO−heme complex; 6c-NO, six-coordinate NO−heme complex; Hb, hemoglobin; H-NOX, heme-nitric oxide and oxygen binding; *Ns* H-NOX, *Nostoc* sp. H-NOX; *Tt* H-NOX, *Thermoanaerobacter tengcongensis* H-NOX; sGC, soluble guanylyl cyclase; $\alpha\beta$I145Y sGC, sGC containing the I145Y mutation in the β subunit; cyt *c*′, cytochrome *c*′; CB, *Clostridium botulinum*; Lb, plant hemoglobins, leghemoglobin; rHb, rice hemoglobin; Asc Hb, invertebrate Hb from *A. suum*; FHb, flavohemoglobins; trHbs, truncated Hbs; trHbN and trHbO, trHbs from *M. tuberculosis*; trCb, single-domain trHb from *C. jejuni*; Ngb, neuroglobin; CLP, chloroperoxidase; PGIS, prostacyclin synthase; HRP, horseradish peroxidase; LPO, lactoperoxidase; EPO, eosinophil peroxidase; CcP, cytochrome *c* peroxidase; MPO, myeloperoxidase; EPR, electron paramagnetic resonance spectroscopy.

REFERENCES

(1) Messerschmidt, A., Huber, R., Poulos, T., and Wieghardt, K., Eds. (2001) *Handbooks of metalloproteins*, Vol. *1*, John Wiley and Sons, Ltd., Chichester, U.K.

(2) Turano, P., and Lu, Y. (2001) Iron in heme and related proteins. In *Handbook on Metalloproteins* (Bertini, I., Sigel, A., and Sigel, H., Eds.) pp 269−342, Marcel Dekker, Inc., New York.

(3) Olson, J. S., and Phillips, G. N. J. (1997) Myoglobin discriminates between O_2, NO, and CO by electrostatic interactions with the bound ligand. *J. Biol. Inorg. Chem. 2*, 544−552.

(4) Walker, F. A. (2005) Nitric oxide interaction with insect nitrophorins and thoughts on the electron configuration of the $\{FeNO\}_6$ complex. *J. Inorg. Biochem. 99*, 216−236.

(5) Dunham, C. M., Dioum, E. M., Tuckerman, J. R., Gonzalez, G., Scott, W. G., and Gilles-Gonzalez, M. A. (2003) A distal arginine in oxygen-sensing heme-PAS domains is essential to ligand binding, signal transduction, and structure. *Biochemistry 42*, 7701−7708.

(6) Aono, S. (2003) Biochemical and biophysical properties of the CO-sensing transcriptional activator CooA. *Acc. Chem. Res. 36*, 825−831.

(7) Derbyshire, E. R., and Marletta, M. A. (2009) Biochemistry of soluble guanylate cyclase. *Handb. Exp. Pharmacol.*,, 17−31.

(8) Zhao, Y., Brandish, P. E., Ballou, D. P., and Marletta, M. A. (1999) A molecular basis for nitric oxide sensing by soluble guanylate cyclase. *Proc. Natl. Acad. Sci. U.S.A. 96*, 14753−14758.

(9) Martin, E., Berka, V., Bogatenkova, E., Murad, F., and Tsai, A. L. (2006) Ligand selectivity of soluble guanylyl cyclase: Effect of the hydrogen bonding tyrosine in the distal heme pocket on binding of oxygen, nitric oxide and carbon monoxide. *J. Biol. Chem. 281*, 27836−27845.

(10) Yeh, H. C., Hsu, P. Y., Wang, J. S., Tsai, A. L., and Wang, L. H. (2005) Characterization of heme environment and mechanism of peroxide bond cleavage in human prostacyclin synthase. *Biochim. Biophys. Acta 1738*, 121−132.

(11) Yeh, H. C., Tsai, A. L., and Wang, L. H. (2007) Reaction mechanisms of 15-hydroperoxyeicosatetraenoic acid catalyzed by human prostacyclin and thromboxane synthases. *Arch. Biochem. Biophys. 461*, 159−168.

(12) Scott, E. E., and Gibson, Q. H. (1997) Ligand migration in sperm whale myoglobin. *Biochemistry 36*, 11909−11917.

(13) Tsai, A. L., Berka, V., Martin, F. E., Ma, X., van den Akker, F., Fabian, M., and Olson, J. S. (2010) Is *Nostoc* H-NOX an NO sensor or Redox Switch? *Biochemistry 49*, 6587−6599.

(14) Rose, E. J., Venkatasubramanian, P. N., Swartz, J. C., Jones, R. D., Basolo, F., and Hoffman, B. M. (1982) Carbon monoxide binding kinetics in "capped" porphyrin compounds. *Proc. Natl. Acad. Sci. U.S.A. 79*, 5742−5745.

(15) Chang, C. K., and Traylor, T. G. (1975) Reversible oxygenation of protoheme-imidazole complex in aqueous solution. *Biochem. Biophys. Res. Commun. 62*, 729−735.

(16) Hoshino, M., Ozawa, K., Seki, H., and Ford, P. C. (1993) Photochemistry of nitric oxide adducts of water-soluble iron(III) porphyrin and ferrihemoproteins studied by nanosecond laser photolysis. *J. Am. Chem. Soc. 115*, 9568−9575.

(17) Carver, T. E., Brantley, R. E. Jr., Singleton, E. W., Arduini, R. M., Quillin, M. L., Phillips, G. N. Jr., and Olson, J. S. (1992) A novel site-directed mutant of myoglobin with an unusually high O_2 affinity and low autooxidation rate. *J. Biol. Chem. 267*, 14443−14450.

(18) Quillin, M. L., Li, T., Olson, J. S., Phillips, G. N. Jr., Dou, Y., Ikeda-Saito, M., Regan, R., Carlson, M., Gibson, Q. H., Li, H., et al. (1995) Structural and functional effects of apolar mutations of the distal valine in myoglobin. *J. Mol. Biol. 245*, 416−436.

(19) Draghi, F., Miele, A. E., Travaglini-Allocatelli, C., Vallone, B., Brunori, M., Gibson, Q. H., and Olson, J. S. (2002) Controlling ligand binding in myoglobin by mutagenesis. *J. Biol. Chem. 277*, 7509−7519.

(20) Stone, J. R., and Marletta, M. A. (1995) The ferrous heme of soluble guanylate cyclase: Formation of hexacoordinate complexes with carbon monoxide and nitrosomethane. *Biochemistry 34*, 16397−16403.

(21) Boon, E. M., Huang, S. H., and Marletta, M. A. (2005) A molecular basis for NO selectivity in soluble guanylate cyclase. *Nat. Chem. Biol. 1*, 53−59.

(22) Stone, J. R., and Marletta, M. A. (1996) Spectral and kinetic studies on the activation of soluble guanylate cyclase by nitric oxide. *Biochemistry 35*, 1093−1099.
(23) Kassner, R. J. (1991) Ligand binding properties of cytochromes c′. *Biochim. Biophys. Acta 1058*, 8−12.
(24) George, S. J., Andrew, C. R., Lawson, D. M., Thorneley, R. N., and Eady, R. R. (2001) Stopped-flow infrared spectroscopy reveals a six-coordinate intermediate in the formation of the proximally bound five-coordinate NO adduct of cytochrome c′. *J. Am. Chem. Soc. 123*, 9683−9684.
(25) Andrew, C. R., George, S. J., Lawson, D. M., and Eady, R. R. (2002) Six- to five-coordinate heme-nitrosyl conversion in cytochrome c′ and its relevance to guanylate cyclase. *Biochemistry 41*, 2353−2360.
(26) Antonyuk, S. V., Rustage, N., Petersen, C. A., Arnst, J. L., Heyes, D. J., Sharma, R., Berry, N. G., Scrutton, N. S., Eady, R. R., Andrew, C. R., and Hasnain, S. S. (2011) Carbon monoxide poisoning is prevented by the energy costs of conformational changes in gas-binding haemproteins. *Proc. Natl. Acad. Sci. U.S.A. 108*, 15780−15785.
(27) Hough, M. A., Antonyuk, S. V., Barbieri, S., Rustage, N., McKay, A. L., Servid, A. E., Eady, R. R., Andrew, C. R., and Hasnain, S. S. (2011) Distal-to-proximal NO conversion in hemoproteins: The role of the proximal pocket. *J. Mol. Biol. 405*, 395−409.
(28) Zhang, W., Olson, J. S., and Phillips, G. N. Jr. (2005) Biophysical and kinetic characterization of HemAT, an aerotaxis receptor from *Bacillus subtilis*. *Biophys. J. 88*, 2801−2814.
(29) Tsai, A.-L. (1994) How does NO activate hemeproteins? *FEBS Lett. 341*, 141−145.
(30) Spiro, T. G., and Jarzecki, A. A. (2001) Heme-based sensors: Theoretical modeling of heme-ligand-protein interactions. *Curr. Opin. Chem. Biol. 5*, 715−723.
(31) Spiro, T. G., Zgierski, M. Z., and Kozlowski, P. M. (2001) Stereoelctronic factors in CO, NO and O_2 binding to heme from vibrational spectroscopy and DFT analysis. *Coord. Chem. Rev. 219−221*, 923−936.
(32) Phillips, G. N. Jr., Teodoro, M. L., Li, T., Smith, B., and Olson, J. S. (1999) Bound CO is a molecular probe of electrostatic potential in the distal pocket of myoglobin. *J. Phys. Chem. B 103*, 8817−8829.
(33) Coyle, C. M., Vogel, K. M., Rush, T. S. III, Kozlowski, P. M., Williams, R., Spiro, T. G., Dou, Y., Ikeda-Saito, M., Olson, J. S., and Zgierski, M. Z. (2003) FeNO structure in distal pocket mutants of myoglobin based on resonance Raman spectroscopy. *Biochemistry 42*, 4896−4903.
(34) Kharitonov, V. G., Russwurm, M., Magde, D., Sharma, V. S., and Koesling, D. (1997) Dissociation of nitric oxide from soluble guanylate cyclase. *Biochem. Biophys. Res. Commun. 239*, 284−286.
(35) Sharma, V. S., Traylor, T. G., Gardiner, R., and Mizukami, H. (1987) Reaction of nitric oxide with heme proteins and model compounds of hemoglobin. *Biochemistry 26*, 3837−3843.
(36) Kharitonov, V. G., Sharma, V. S., Magde, D., and Koesling, D. (1997) Kinetics of nitric oxide dissociation from five- and six-coordinate nitrosyl hemes and heme proteins, including soluble guanylate cyclase. *Biochemistry 36*, 6814−6818.
(37) Franzen, S. (2002) Spin-dependent mechanism for diatomic ligand binding to heme. *Proc. Natl. Acad. Sci. U.S.A. 99*, 16754−16759.
(38) Strickland, N., and Harvey, J. N. (2007) Spin-forbidden ligand binding to the ferrous-heme group: Ab initio and DFT studies. *J. Phys. Chem. B 111*, 841−852.
(39) Harvey, J. N. (2000) DFT computation of the intrinsic barrier to CO geminate recombination with heme compounds. *J. Am. Chem. Soc. 122*, 12401−12402.
(40) Ionascu, D., Gruia, F., Ye, X., Yu, A., Rosca, F., Beck, C., Demidov, A., Olson, J. S., and Champion, P. M. (2005) Temperature-dependent studies of NO recombination to heme and heme proteins. *J. Am. Chem. Soc. 127*, 16921−16934.
(41) Olson, J. S., and Phillips, G. N. Jr. (1996) Kinetic Pathways and Barriers for Ligand Binding to Myoglobin. *J. Biol. Chem. 271*, 17596.
(42) Dou, Y., Maillett, D. H., Eich, R. F., and Olson, J. S. (2002) Myoglobin as a model system for designing heme protein based blood substitutes. *Biophys. Chem. 98*, 127−148.
(43) Eich, R. F. (1997) Reactions of Nitric Oxide with Myoglobin. In *Biochemistry and Cell Biology*, Rice University, Houston.
(44) Foley, E. W. (2005) Physiologically Relevant Reactions of Myoglobin and Hemoglobin with NO. In *Biochemistry and Cell Biology*, Rice University, Houston.
(45) Coyle, C. M., Puranik, M., Youn, H., Nielsen, S. B., Williams, R. D., Kerby, R. L., Roberts, G. P., and Spiro, T. G. (2003) Activation mechanism of the CO sensor CooA. Mutational and resonance Raman spectroscopic studies. *J. Biol. Chem. 278*, 35384−35393.
(46) Hargrove, M. S., Barry, J. K., Brucker, E. A., Berry, M. B., Phillips, G. N. Jr., Olson, J. S., Arredondo-Peter, R., Dean, J. M., Klucas, R. V., and Sarath, G. (1997) Characterization of recombinant soybean leghemoglobin a and apolar distal histidine mutants. *J. Mol. Biol. 266*, 1032−1042.
(47) Arredondo-Peter, R., Hargrove, M. S., Sarath, G., Moran, J. F., Lohrman, J., Olson, J. S., and Klucas, R. V. (1997) Rice hemoglobins. Gene cloning, analysis, and O_2-binding kinetics of a recombinant protein synthesized in *Escherichia coli*. *Plant Physiol. 115*, 1259−1266.
(48) Lu, C., Egawa, T., Mukai, M., Poole, R. K., and Yeh, S. R. (2008) Hemoglobins from *Mycobacterium tuberculosis* and *Campylobacter jejuni*: A comparative study with resonance Raman spectroscopy. *Methods Enzymol. 437*, 255−286.
(49) Van Doorslaer, S., Dewilde, S., Kiger, L., Nistor, S. V., Goovaerts, E., Marden, M. C., and Moens, L. (2003) Nitric oxide binding properties of neuroglobin. A characterization by EPR and flash photolysis. *J. Biol. Chem. 278*, 4919−4925.
(50) Abu-Soud, H. M., Gachhui, R., Raushel, F. M., and Stuehr, D. J. (1997) The ferrous-dioxy complex of neuronal nitric oxide synthase. Divergent effects of L-arginine and tetrahydrobiopterin on its stability. *J. Biol. Chem. 272*, 17349−17353.
(51) Abu-Soud, H. M., Wu, C., Ghosh, D. K., and Stuehr, D. J. (1998) Stopped-flow analysis of CO and NO binding to inducible nitric oxide synthase. *Biochemistry 37*, 3777−3786.
(52) Franke, A., Stochel, G., Jung, C., and Van Eldik, R. (2004) Substrate binding favors enhanced NO binding to P450cam. *J. Am. Chem. Soc. 126*, 4181−4191.
(53) Gerber, N. C., and Sligar, S. G. (1992) Catalytic mechanism of cytochrome P-450: Evidence for a distal charge relay. *J. Am. Chem. Soc. 114*, 8742−8743.
(54) Sevrioukova, I. F., and Peterson, J. A. (1995) Reaction of carbon monoxide and molecular oxygen with P450terp (CYP108) and P450BM-3 (CYP102). *Arch. Biochem. Biophys. 317*, 397−404.
(55) Quaroni, L. G., Seward, H. E., McLean, K. J., Girvan, H. M., Ost, T. W., Noble, M. A., Kelly, S. M., Price, N. C., Cheesman, M. R., Smith, W. E., and Munro, A. W. (2004) Interaction of nitric oxide with cytochrome P450 BM3. *Biochemistry 43*, 16416−16431.
(56) Lambeir, A. M., and Dunford, H. B. (1985) Oxygen binding to dithionite-reduced chloroperoxidase. *Eur. J. Biochem. 147*, 93−96.
(57) Lange, R., Heiber-Langer, I., Bonfils, C., Fabre, I., Negishi, M., and Balny, C. (1994) Activation volume and energetic properties of the binding of CO to hemoproteins. *Biophys. J. 66*, 89−98.
(58) Yeh, H. C., Hsu, P. Y., Tsai, A. L., and Wang, L. H. (2008) Spectroscopic characterization of the oxyferrous complex of prostacyclin synthase in solution and in trapped sol-gel matrix. *FEBS J. 275*, 2305−2314.
(59) Yeh, H. C., Hsu, P. Y., Wang, J. S., Tsai, A. L., and Wang, L. H. (2005) Characterization of heme environment and mechanism of peroxide bond cleavage in human prostacyclin synthase. *Biochim. Biophys. Acta 1738*, 121−132.
(60) Coletta, M., Ascoli, F., Brunori, M., and Traylor, T. G. (1986) pH dependence of carbon monoxide binding to ferrous horseradish peroxidase. *J. Biol. Chem. 261*, 9811−9814.
(61) Rodriguez-Lopez, J. N., Smith, A. T., and Thorneley, R. N. (1997) Effect of distal cavity mutations on the binding and activation of oxygen by ferrous horseradish peroxidase. *J. Biol. Chem. 272*, 389−395.
(62) Abu-Soud, H. M., and Hazen, S. L. (2001) Interrogation of heme pocket environment of mammalian peroxidases with diatomic ligands. *Biochemistry 40*, 10747−10755.

(63) Galijasevic, S., Saed, G. M., Diamond, M. P., and Abu-Soud, H. M. (2004) High dissociation rate constant of ferrous-dioxy complex linked to the catalase-like activity in lactoperoxidase. *J. Biol. Chem. 279*, 39465−39470.
(64) Babcock, G. T., and Wikstrom, M. (1992) Oxygen activation and the conservation of energy in cell respiration. *Nature 356*, 301−309.
(65) Mims, M. P., Porras, A. G., Olson, J. S., Noble, R. W., and Peterson, J. A. (1983) Ligand binding to heme proteins. An evaluation of distal effects. *J. Biol. Chem. 258*, 14219−14232.
(66) Jantschko, W., Furtmuller, P. G., Zederbauer, M., Jakopitsch, C., and Obinger, C. (2004) Kinetics of oxygen binding to ferrous myeloperoxidase. *Arch. Biochem. Biophys. 426*, 91−97.
(67) Murphy, E. J., Marechal, A., Segal, A. W., and Rich, P. R. (2010) CO binding and ligand discrimination in human myeloperoxidase. *Biochemistry 49*, 2150−2158.
(68) Collman, J. P., Boulatov, R., Sunderland, C. J., and Fu, L. (2004) Functional analogues of cytochrome c oxidase, myoglobin, and hemoglobin. *Chem. Rev. 104*, 561−588.
(69) Collman, J. P., and Reed, C. A. (1973) Syntheses of ferrous-porphyrin complexes. A hypothetical model for deoxymyoglobin. *J. Am. Chem. Soc. 95*, 2048−2049.
(70) Ford, P. C., and Lorkovic, I. M. (2002) Mechanistic aspects of the reactions of nitric oxide with transition-metal complexes. *Chem. Rev. 102*, 993−1018.
(71) Tani, F., Matsu-ura, M., Ariyama, K., Setoyama, T., Shimada, T., Kobayashi, S., Hayashi, T., Matsuo, T., Hisaeda, Y., and Naruta, Y. (2003) Iron twin-coronet porphyrins as models of myoglobin and hemoglobin: Amphibious electrostatic effects of overhanging hydroxyl groups for successful CO/O_2 discrimination. *Chemistry 9*, 862−870.
(72) Chang, C. K., and Traylor, T. G. (1975) Kinetics of oxygen and carbon monoxide binding to synthetic analogs of the myoglobin and hemoglobin active sites. *Proc. Natl. Acad. Sci. U.S.A. 72*, 1166−1170.
(73) Collman, J. P., Brauman, J. I., Iverson, B. L., Sessler, J. L., Morris, R. M., and Gibson, Q. H. (1983) O_2 and CO binding to iron(II) porphyrins: A comparison of the "picket fence" and "pocket" porphyrins. *J. Am. Chem. Soc. 105*, 3052−3064.
(74) Shantha, D., James, B. R., Dolphin, D., Traylor, T. G., and Lopez, M. A. (1994) Dioxygen and carbon monoxide binding to apolar cyclophane hemes: Durene-capped hemes. *J. Am. Chem. Soc. 116*, 6−14.
(75) Tetreau, C., Lavalette, D., Momenteau, M., Fischer, J., and Weiss, R. (1994) Structure-reactivity relationship in oxygen and carbon monoxide binding with some heme models. *J. Am. Chem. Soc. 116*, 11840−11848.
(76) Smagghe, B. J., Halder, P., and Hargrove, M. S. (2008) Measurement of distal histidine coordination equilibrium and kinetics in hexacoordinate hemoglobins. *Methods Enzymol. 436*, 359−378.
(77) Eich, R. F., Li, T., Lemon, D. D., Doherty, D. H., Curry, S. R., Aitken, J. F., Mathews, A. J., Johnson, K. A., Smith, R. D., Phillips, G. N. Jr., and Olson, J. S. (1996) Mechanism of NO-induced oxidation of myoglobin and hemoglobin. *Biochemistry 35*, 6976−6983.
(78) Gardner, P. R., Gardner, A. M., Brashear, W. T., Suzuki, T., Hvitved, A. N., Setchell, K. D., and Olson, J. S. (2006) Hemoglobins dioxygenate nitric oxide with high fidelity. *J. Inorg. Biochem. 100*, 542−550.
(79) Tsai, A. L., Berka, V., Sharina, I., and Martin, E. (2011) Dynamic ligand exchange in soluble guanylyl cyclase: Implications for sGC regulation and desensitization. *J. Biol. Chem.*, in press.
(80) Kruglik, S. G., Lambry, J.-C., Ciannetti, S., Martin, J.-L., Eady, R. R., Andrew, C. R., and Negrerie, M. (2007) Molecular basis for nitric oxide dynamics and affinity with Alcaligenes xylosoxidans cytochrome *c'*. *J. Biol. Chem. 282*, 5053−5062.